

Investigation of the $^{10}\text{B}(p, \alpha)^7\text{Be}$ reaction from 0.8 to 2.0 MeV

B. Vande Kolk,¹ K. T. Macon,^{1,2,*} R. J. deBoer[Ⓞ],¹ T. Anderson,¹ A. Boeltzig,^{1,†} K. Brandenburg,³ C. R. Brune,³ Y. Chen,¹ A. M. Clark,¹ T. Danley,³ B. Frentz,¹ R. Giri,³ J. Görres,¹ M. Hall,¹ S. L. Henderson,¹ E. Holmbeck,¹ K. B. Howard,¹ D. Jacobs,³ J. Lai,¹ Q. Liu,¹ J. Long,¹ K. Manukyan,¹ T. Massey,³ M. Moran,¹ L. Morales,¹ D. Odell,³ P. O'Malley,¹ S. N. Paneru,³ A. Richard,³ D. Schneider,⁴ M. Skulski,¹ N. Sensharma,¹ C. Seymour,¹ G. Seymour,¹ D. Soltész,³ S. Strauss,¹ A. Voinov,³ L. Wüstrich,^{1,‡} and M. Wiescher¹

¹Department of Physics and The Joint Institute for Nuclear Astrophysics, University of Notre Dame, Notre Dame, Indiana 46556, USA

²Department of Physics and Astronomy, Louisiana State University, Baton Rouge, Louisiana 70803, USA

³Edwards Accelerator Laboratory, Department of Physics and Astronomy, Ohio University, Athens, Ohio 45701, USA

⁴Lawrence Livermore National Laboratory, Livermore, California 94550, USA



(Received 18 January 2022; accepted 26 April 2022; published 11 May 2022)

Background: A multitude of broad interfering resonances characterize the $^{10}\text{B}(p, \alpha)^7\text{Be}$ cross section at low energies. The complexity of the reaction mechanism, as well as conflicting experimental measurements, have so far prevented a reliable prediction of the cross section over the energy ranges pertinent for a boron-proton fusion reactor environment.

Purpose: To improve the evaluated cross section of the $^{10}\text{B}(p, \alpha)^7\text{Be}$ reaction, this study targets the proton energy region from 0.8 to 2.0 MeV, where kinematic overlap of the scattered protons and reaction α particles have made past measurements very challenging.

Method: New detailed studies of the reaction have been performed at the Edwards Accelerator Laboratory at Ohio University and the Nuclear Science Laboratory at the University of Notre Dame using time-of-flight and degrader foil techniques, respectively.

Results: Proton and α -particle signals were clearly resolved using both techniques, and 16 point differential cross sections were measured over an angular range of $\theta_{\text{lab}} = 45^\circ$ and 157.5° . A comprehensive R -matrix analysis of the experimental data, including data from previous low-energy studies of the $^{10}\text{B}(p, \alpha)^7\text{Be}$, $^{10}\text{B}(p, p)^{10}\text{B}$, and $^{10}\text{B}(p, \gamma)^{11}\text{C}$ reactions, was achieved over the region of measurement. Using a representative set of previous data, the fit was extended to very low energies.

Conclusions: On the basis of this data and R -matrix analysis, a more reliable and consistent description of the $^{10}\text{B}(p, \alpha)^7\text{Be}$ cross section has been established. The uncertainty over the energy range of this study has been reduced from $\approx 20\%$ to $\approx 10\%$, and the level structure over this region has been clarified considerably.

DOI: [10.1103/PhysRevC.105.055802](https://doi.org/10.1103/PhysRevC.105.055802)

I. INTRODUCTION

Aneutronic plasma fusion systems have been increasingly discussed as possible energy sources that would avoid the disadvantage of long-lived radioactive end-products [1]. The most frequently quoted aneutronic sources are the $^3\text{He}(^3\text{He}, 2p)^4\text{He}$ ($Q = 12.9$ MeV) and the $^{11}\text{B}(p, 2\alpha)^4\text{He}$ ($Q = 8.7$ MeV) reactions, with helium as the primary end-product along with a sufficient amount of energy generation. Of particular interest is the $^{11}\text{B}(p, 2\alpha)^4\text{He}$ process [2] because, unlike ^3He , being mostly produced as a decay product of tritium ^3H [3], ^{11}B is considered to be a naturally abundant and inexpensive fuel stock. While the $^{11}\text{B} + p$ fusion system

has already been considered earlier as a potential energy source in traditional plasma systems [4,5], or for colliding beam reactors [6], recent observations of aneutronic fusion reactions on laser-picosecond plasmas [7] have motivated the discussion of possible applications for $^{11}\text{B}(p, 2\alpha)^4\text{He}$ in laser-driven, hot-pulsed plasma systems [8–11]. In particular, the development of high power petawatt laser systems with picosecond durations [12,13] opens up new windows of application. The optimal energy range for the $^{11}\text{B} + p$ fusion system is between 200 and 1000 keV because of a broad resonance structure observed at 600 keV center of mass energy [14] that dominates the total cross section of the reaction. Therefore, the efforts of laser-driven fusion studies focus on that energy range [15].

The $^{11}\text{B}(p, 2\alpha)^4\text{He}$ fusion reaction does not produce any long-lived radioactive products; however, the 19% ^{10}B abundance in naturally occurring boron fuel material will produce the longer-lived ^7Be isotope through the $^{10}\text{B}(p, \alpha)^7\text{Be}$ reaction. ^7Be decays by electron capture with a laboratory lifetime of 53.2 d under emission of a characteristic 457 keV γ line from the 10% transition to the first excited state in

*Present address: InstroTek, 1 Triangle Drive, P.O. Box 13944, Research Triangle Park, NC 27709.

†Present address: Helmholtz-Zentrum Dresden-Rossendorf (HZDR), Bautzner Landstraße 400, 01328 Dresden, Germany.

‡Present address: Technical University of Munich, Arcisstraße 21, 80333 Munich, Germany.

${}^7\text{Li}$ with subsequent γ decay to the ground state [16]. The total cross section of the reaction near 600 keV is 10 mb according to the EXFOR data compilation [17]. This value is substantially lower than the 1 barn cross section reported for the ${}^{11}\text{B}(p, 2\alpha){}^4\text{He}$ reaction [14]. The production of spurious amounts of ${}^7\text{Be}$ in a plasma fusion operation with enriched ${}^{11}\text{B}$ fuel may therefore not be a matter of great concern, but the observation of ${}^7\text{Be}$ from a boron-hydrogen plasma burning environment, doped with a well know amount of ${}^{10}\text{B}$, may provide the means for temperature determination in the plasma region.

This may provide an independent test for temperature analysis in the new generation of laser-driven, hot-plasma facilities such as the National Ignition Facility (NIF) [18] or OMEGA [19], where recent studies of d - t and d - d fusion signals indicated considerable uncertainty in the temperature analysis [20]. Yet, the EXFOR data compilation indicates significant differences and uncertainties between the different data sets for the possible transitions to the ground state ${}^{10}\text{B}(p, \alpha_0){}^7\text{Be}$ and the first excited state ${}^{10}\text{B}(p, \alpha_1){}^7\text{Be}^*$ in ${}^7\text{Be}$ (see Wiescher *et al.* [21]). The ground state transition has been measured extensively in the low energy range between 100 keV and 1 MeV [21–32], with some experiments covering a higher energy range up to 2 MeV [24,26]. More recent efforts using the Trojan horse method (THM) have concentrated on the study of very low energies [33–36]. The ${}^{10}\text{B}(p, \alpha_1){}^7\text{Be}^*$ channel has been measured independently either by particle spectroscopy [24,26] or by γ -ray spectroscopy using the ${}^{10}\text{B}(p, \alpha_1 - \gamma){}^7\text{Be}$ channel [21,24,37–39]. The discrepancies are most visible in the energy range of interest for the ${}^{11}\text{B}(p, 2\alpha){}^4\text{He}$ around 600 keV. To use the ${}^{10}\text{B}(p, \alpha){}^7\text{Be}$ reaction as a monitor, the cross section needs to be known with high accuracy and the presently existing uncertainties need to be removed.

The very low energies accessed at NIF remain below the energy range of accelerator-based measurements, and THM measurements have relatively large, model dependent, uncertainties [36]. Therefore, to determine the low-energy cross section, the phenomenological R -matrix approach has often been utilized to extrapolate from higher energies that are experimentally accessible [40,41]. The extrapolation is accomplished by constraining the phenomenological model with higher energy cross section data and level information from nuclear structure studies. For the ${}^{10}\text{B}(p, \alpha){}^7\text{Be}$ reaction, this approach is complicated by inconsistent cross section measurements and incomplete level structure information (see Fig. 1). The experimental data often have large discrepancies in the absolute scale of the cross section and in some cases even the energy dependence of data sets are inconsistent, as recently highlighted in Wiescher *et al.* [21].

One of the main conclusions of Wiescher *et al.* [21] was that the current data do not place sufficient constraints on the broad resonance contributions in the R -matrix description of the ${}^{10}\text{B} + p$ reactions. This is emphasized by the rather different R -matrix fits obtained in the recent works [21,31,32,36], despite the use of similar experimental data for the fits. One chief reason for this is that the reaction kinematics result in very similar energies for the α particles and protons from

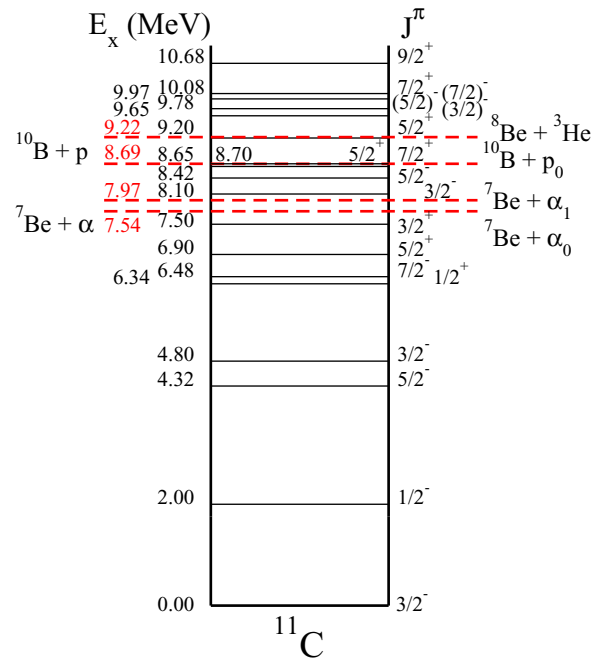


FIG. 1. Level diagram of the ${}^{11}\text{C}$ system up to $E_x \approx 11$ MeV as given in the Evaluated Nuclear Structure Data File (ENSDF) evaluation [42]. The red dashed lines indicate particle separation energies.

the ${}^{10}\text{B}(p, \alpha_0){}^7\text{Be}$ and ${}^{10}\text{B}(p, p_0){}^{10}\text{B}$ reactions, respectively. With standard resolution (≈ 20 keV) silicon detectors at room temperature, it is very difficult to separate the α -particle and proton peaks from about 0.8 to 2 MeV (see Fig. 2) laboratory proton energy (E_p). In addition, the emitted particles are too low in energy for particle identification through energy loss techniques, using an E - ΔE telescope for example. Hence the data available in the literature over this energy region are quite limited.

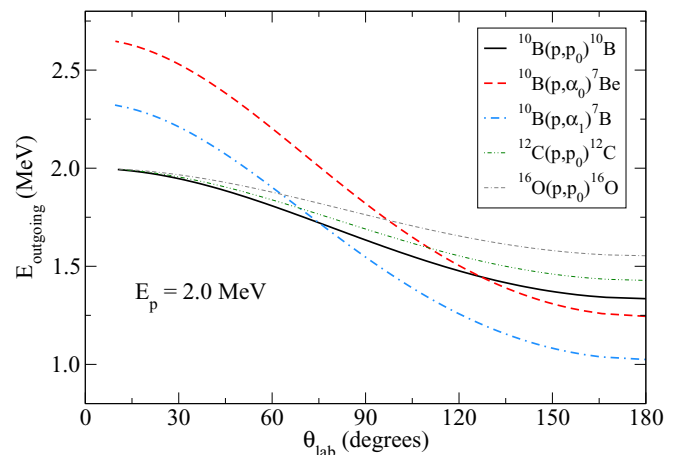


FIG. 2. Energies of outgoing particles for ${}^{10}\text{B} + p$ and ${}^{12}\text{C}(p, p)$ and ${}^{16}\text{O}(p, p)$ reactions at $E_p = 2.0$ MeV. The similar outgoing particle energies over the central angular range complicates measurements from $E_p = 0.8$ to 3.0 MeV.

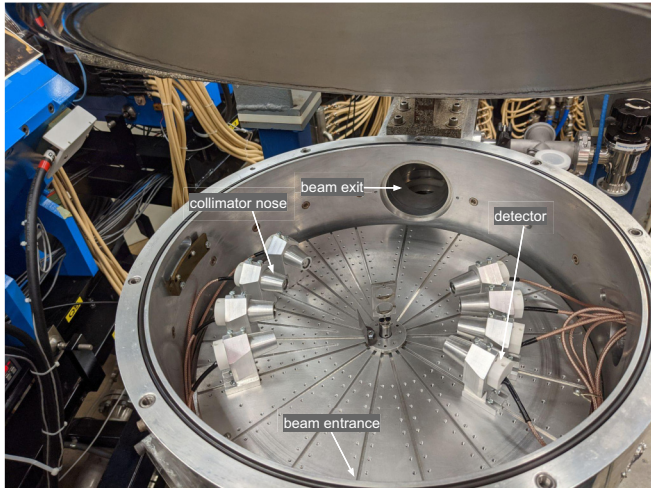


FIG. 3. Notre Dame experimental setup. See text for details.

In this work, we report new experimental differential cross section measurements of the $^{10}\text{B}(p, \alpha_0)^7\text{Be}$ and $^{10}\text{B}(p, \alpha_1)^7\text{Be}$, reactions from $E_p = 0.8$ to 2 MeV. In Sec. II two experimental setups at the University of Notre Dame and Ohio University are described and in Sec. III the experimental yields and absolute cross sections are reported. The multi-channel R -matrix analysis is discussed in Sec. IV and the effect on the reaction rates in Sec. V. Summarizing remarks are made in Sec. VI.

II. EXPERIMENTAL SETUP

Two experimental setups, at two different experimental facilities, were used for new cross section measurements of the $^{10}\text{B}(p, \alpha_0)^7\text{Be}$, $^{10}\text{B}(p, \alpha_1)^7\text{Be}$, and $^{10}\text{B}(p, p)^{10}\text{B}$ reactions. Measurements were made at the University of Notre Dame (UND) Nuclear Science Laboratory (NSL) using a degrader foil method, while those at the Edwards Accelerator Laboratory at Ohio University (OU) were performed using the time-of-flight (ToF) technique. Additional details can be found in the Ph.D. thesis of Vande Kolk [43].

A. Notre Dame setup

For the experimental measurements at the UND NSL, the 5 MV Stable Ion Accelerator for Nuclear Astrophysics (St. ANA) was used to produce proton beams between 0.8 and 2.0 MeV. The energy calibration of the beam was determined using the energies of well known resonances in the $^{27}\text{Al}(p, \gamma)^{28}\text{Si}$ reaction [44], and was determined to better than 1 keV over the energy range of the present measurements. Beam intensities between 100 and 150 nA were used and read from an electrically isolated beam stop. The measurements were made using a 43 cm diameter ORTEC scattering chamber as shown in Fig. 3. The chamber was equipped with a double beam collimator just before the entrance to the chamber, which was used to define the beam spot on target to ≈ 1.27 cm diameter. The beam stop was located ≈ 0.61 m downstream of the target position and the exit port of the chamber was collimated to limit background from back-

scattering off the beam stop. Eight S3590 Hamamatsu PIN photodiodes (bare chip type, 10×10 mm, 300 μm thickness, biased to +50 V), placed at $\theta_{\text{lab}} = 45, 65, 75, 85, 95, 105, 115,$ and 135° were used for charged particle detection. The Hamamatsu particle detectors were mounted in custom housings and were doubly collimated. A 0.63 cm collimator was placed directly in front of the detector, while the second, of a smaller diameter, was mounted at the end of a conical nose piece of either 0.25 or 0.30 cm in length. These collimators were made of varying sizes (ranging from 0.13 to 0.51 cm), decreasing in diameter from backward to forward angle, to achieve a similar count rate in each detector. The target was placed at a 45° angle relative to the incoming beam, allowing for the placement of a set of detectors at both forward and backward angles. The more forward set of detectors were placed at a distance of 14.3 cm from the target, while those at backward angles were placed at a distance of 10.7 cm. This resulted in detection solid angles ranging from 6.7×10^{-5} to 6.5×10^{-4} sr.

As boron targets of the desired thickness are not self-supporting, targets were prepared by evaporating enriched ^{10}B powder (96%) onto thin ($\approx 3.6 \mu\text{m}/\text{cm}^2$), self-supporting, carbon foils. The evaporation was performed at the NSL, producing ^{10}B layers of 5.0(5) $\mu\text{g}/\text{cm}^2$. The carbon foils did provide an additional source of background from proton elastic scattering. Additional reactions on carbon were not energetically allowed.

Figure 2 shows the energies of the scattered protons and α particles from the $^{10}\text{B} + p$ reactions at $E_p = 2.0$ MeV as well as background reactions from $^{12}\text{C}(p, p)^{12}\text{C}$ and $^{16}\text{O}(p, p)^{16}\text{O}$. The carbon background comes mainly from the thin carbon backing, but also is present from beam induced carbon build up on the target. Oxygen contamination is present from moisture in the carbon foil and from oxidization and nitrogen contamination in the boron target.

In order to separate α -particle events from those of proton produced by elastic scattering, a $250 \mu\text{m}/\text{cm}^2$ carbon degrader foil was placed in front of each detector. Since the stopping cross section for protons is considerably less than that of α particles in the degrader foil, the α -particle peaks are shifted by a greater amount downward in energy. The thickness of $250 \mu\text{g}/\text{cm}^2$ was chosen as it was found to shift the α peaks downward enough in energy to separate them from the proton scattering peaks, but still leave them with enough energy to be above the detector thresholds (≈ 400 keV). Example energy spectra for the same incoming beam energy ($E_p = 2.0$ MeV) but with and without the degrader foil are shown in Fig. 4.

The electronics for each detector consisted of a Canberra model 2003B preamplifier, an Ortec 671 spectroscopic amplifier (3 μs shaping time), and finally a Canberra 8715 analog-to-digital converter (ADC). The ADCs were read into a FAST ComTec Base Module MPA-3 data acquisition system.

B. Ohio university setup

Proton beams of between 20 and 100 nA were delivered to the target by the OU 4.5 MeV T-type tandem Pelletron

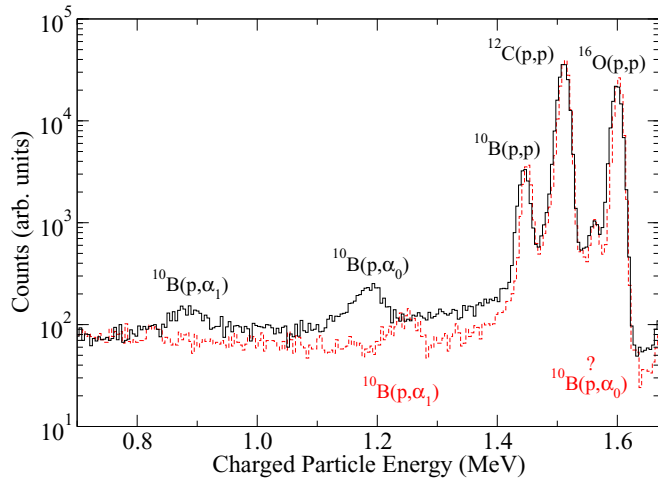


FIG. 4. Example energy spectra for $E_p = 2.0$ MeV at $\theta_{\text{lab}} = 115^\circ$ on a boron transmission target with thin self-supporting carbon backing with (solid black line) and without (red dashed line) a $250 \mu\text{g}/\text{cm}^2$ carbon degrader foil. Without the degrader foil, the α -particle peak from the $^{10}\text{B}(p, \alpha_0)^7\text{Be}$ reaction is obscured beneath the elastic proton scattering peaks.

accelerator. The proton beam was produced with 200 ns between bunches. A scattering chamber, customized for ToF-type experiments, was utilized. A detailed description of the chamber can be found in Wheeler [45]. Eight ORTEC silicon detectors [model no. (B)U-013-100-100] were used for charge particle detection. In order to achieve sufficient ToF resolution, the three detectors at the most forward angles were placed at a distance of 1.0 m from the target, while the

remainder were placed at 0.30 m. This provided sufficient ToF resolution for the proton and α -particle events to be clearly distinguishable. Detectors were doubly collimated, with the first collimator (diameter of 1.27 cm) located near the edge of the scattering chamber at a distance of 13 cm from the target, while the second collimator (diameter of 1.67 cm) was placed directly in front of the detector. The detectors were positioned at angles of $\theta_{\text{lab}} = 52.5, 67.5, 82.5, 97.5, 112.5, 127.5, 142.5,$ and 157.5° . Detector solid angles varied from 2.4×10^{-4} to 3.5×10^{-3} sr. For a clear view of the target with each detector, the target was positioned at an angle of 30° from perpendicular to the incoming beam direction. The experimental setup is shown in Fig. 5.

Boron targets were produced in a similar manner as those described in Sec. II A, but with a higher enrichment of 99% in ^{10}B . The target thicknesses were determined using an energy loss setup and a radioactive α source. Stopping cross sections were taken from SRIM-2013 [46]. In addition, the thickness was also determined during the peak fitting process of the experimental $^{10}\text{B}(p, \alpha)^7\text{Be}$ yields. A single target was used for all experimental measurements at OU and was found to have a thin carbon backing of $5.8(3) \mu\text{g}/\text{cm}^2$ and a boron thickness of $53(3) \mu\text{g}/\text{cm}^2$.

III. DATA ANALYSIS

A. Notre Dame data

Figure 4 shows a typical spectrum from the measurements at the University of Notre Dame described in Sec. II A. Because of the significant amount of straggling suffered by the protons and α particles through the degrader foil, peak yields were determined by modeling the peak shapes with an

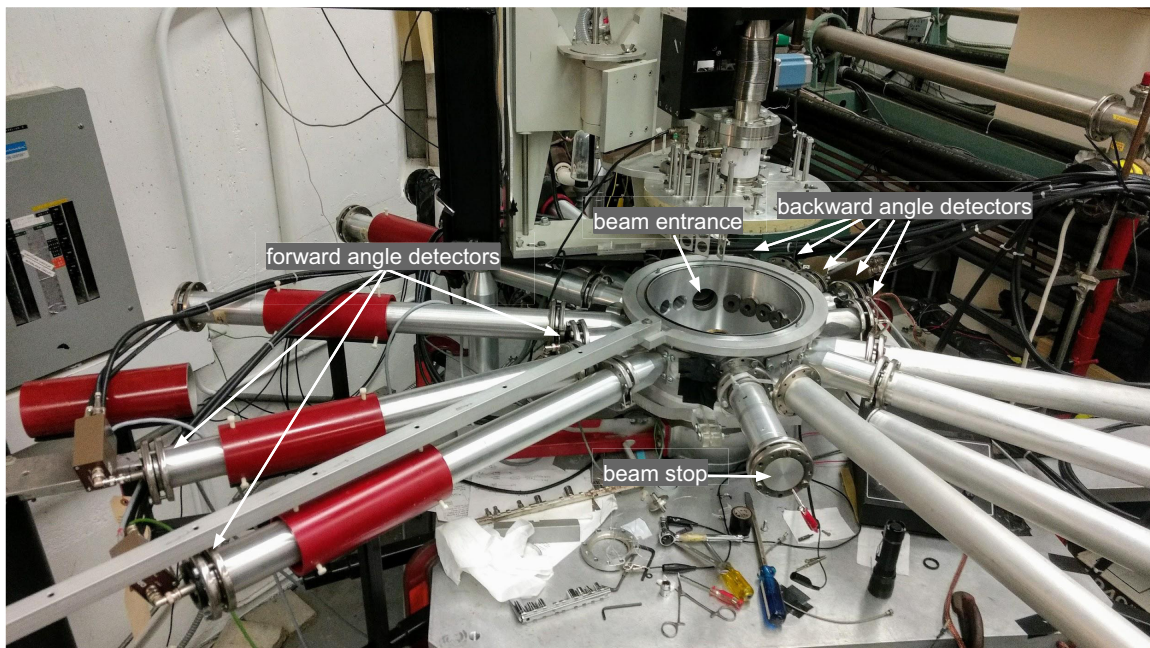


FIG. 5. Ohio University experimental setup. Particle detectors were placed at the end of the extension pipes that have been installed off of the main section of the scattering chamber. The larger distance between detector and target is required in order to provide sufficient resolution for particle identification using ToF. See text for details.

TABLE I. Summary of systematic uncertainty estimates.

Systematic uncertainty contribution	%
University of Notre Dame	
^{10}B target thickness	10
Target degradation	5
Beam current reading	3
Total	12
Ohio University	
^{10}B target thickness	6
^{12}C target thickness	5
systematic uncertainty from Meyer <i>et al.</i> [48]	3
R -matrix interpolation	5
Total	10

exponentially modified Gaussian and linear background term. As discussed in Sec. II A the number of protons that impinged on the target were determined by reading the current from an electrically isolated beam stop. The uncertainty in charge reading was found to be within 3%. The deadtime produced by proton scattering determined the beam intensity limit and was kept below 2%. This allowed a determination of the number of protons that impinged on the target (N_p) to with 3% uncertainty.

Target stability studies were performed prior to the experimental data run. From repeated measurements of the yield at the same energy, it was found that very limited target deterioration occurred if beam intensities were kept below 200 nA. Thus, to be conservative, the measurements were performed with beam intensities below 150 nA. However, given the rather thin target (see Sec. II A), a systematic uncertainty of 5% was added to the overall uncertainty budget (see Table I).

The efficiency of each detector in the setup (ϵ) was determined using two methods: geometric measurement and yield measurements from the well known angular distribution of the $E_p = 1366$ keV resonance in the $^{27}\text{Al}(p, \alpha_0)^{24}\text{Mg}$ reaction [47]. The reaction produces a nearly isotropic distribution of α particles (in the center of mass frame), with angular distribution coefficients of $a_2 = -0.08(2)$ and $a_4 = 0.00(2)$. The two methods were found to agree to within uncertainties, giving an uncertainty in the relative angular distributions of 3%. The absolute differential cross section, assuming a thin target, can then be calculated by

$$\frac{d\sigma}{d\Omega_X} = A_X N_p N_B \epsilon, \quad (1)$$

where the index X denotes either the $^{10}\text{B}(p, \alpha_0)^7\text{Be}$ or $^{10}\text{B}(p, \alpha_1)^7\text{Be}$ reaction, $\frac{d\sigma}{d\Omega}$ is the differential cross section, A is the area of the peak from the charged particle spectrum, N_p are the number of protons made incident on the target, N_B are the number of boron atoms per unit area in the target, and ϵ is the efficiency. Due to the very thin target (see Sec. II A) and the changes in the cross section as a function of energy, energy loss corrections (less than 1.25 keV) were negligible compared with the experimental uncertainties.

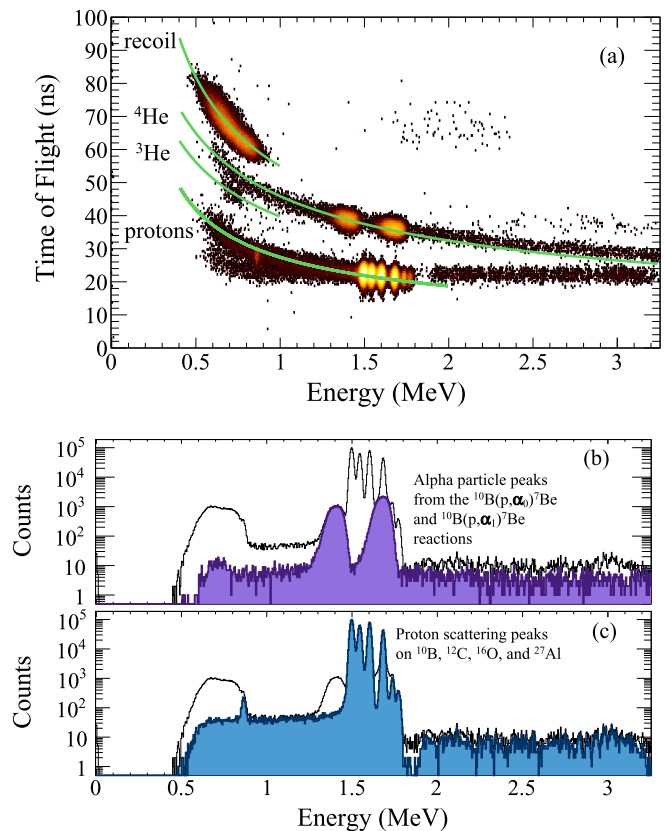


FIG. 6. ToF charged-particle spectra with the setup shown in Fig. 5 for $E_p = 1.9$ MeV at 82.5 degrees. The green curves in (a) indicate the kinematic curves for protons, ^3He , ^4He , and heavy recoils. (b) and (c) indicate the spectra obtained by gating on the α -particle (purple) and proton (blue) curves. The ungated spectrum is also indicated for comparison. In (b), the two large, broad peaks correspond to the α -particles coming from the $^{10}\text{B}(p, \alpha_0)^7\text{Be}$ (higher energy) and $^{10}\text{B}(p, \alpha_1)^7\text{Be}$ (lower energy). In (c), the cluster of proton scattering peaks around 1.5 MeV correspond to ^{10}B , ^{12}C , ^{16}O , and ^{27}Al (from lowest to highest energy). The smaller peak at about 0.8 MeV corresponds to inelastic proton scattering from the first excited state of ^{10}B . The flat background at higher energies comes from multiple scattering off of upstream beam line components.

B. Ohio university data

Figure 6(a) shows a typical ToF-versus-energy spectrum. As described in Sec. II B, the target-to-detector flight path provided sufficient resolution to distinguish clearly the different types of particles. Starting from the bottom of the figure, the four kinematic curves correspond to protons, ^3He , ^4He , and heavy recoils. Gating on the α -particle curve results in the purple spectrum shown in Fig. 6(b), while gating on the proton curve results in the blue spectrum shown in Fig. 6(c). In both cases, the ungated spectrum is also indicated for comparison.

The relative efficiency of the setup was determined by geometric measurement and by comparison with the well-known scattering cross section of the $^{12}\text{C}(p, p)^{12}\text{C}$ reaction [48]. The phenomenological R -matrix fit described in Azuma *et al.* [49] was used to interpolate the differential cross section from the angles of measurement by Meyer *et al.* [48] to those of the

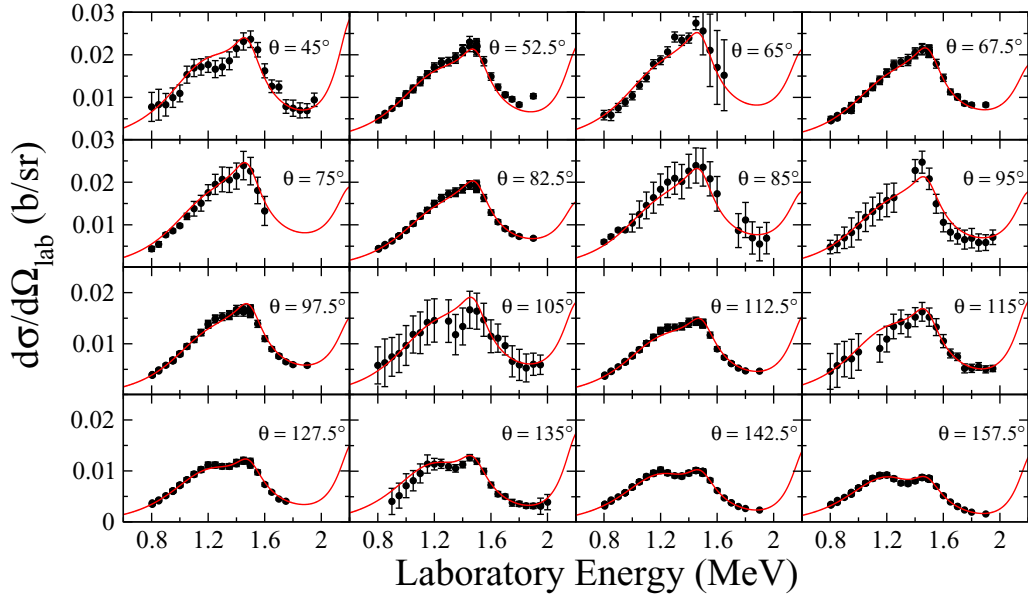


FIG. 7. Experimental measurements of the $^{10}\text{B}(p, \alpha_0)^7\text{Be}$ reaction from the present work. The Notre Dame data were measured at whole angles, while those at OU at half-angles. The red solid line indicates the R -matrix fit described in Sec. IV. All quantities are in the laboratory frame of reference. For comparison with figures later in the text that are given in the center of mass frame, the energy scale should be multiplied by a factor of ≈ 10 or 11.

present experiment. Sensitivity tests found that variations of up to 5% were observed in the calculations, in addition to the 3% systematic uncertainty quoted by Meyer *et al.* [48].

A complication in the measurement arose from unreliable current readings from the beam stop. As the individual scattering peaks were resolvable at most of the energies and angles of measurement, the $^{10}\text{B}(p, \alpha_0)^7\text{Be}$ and $^{10}\text{B}(p, \alpha_1)^7\text{Be}$ differential cross sections were determined relative to the $^{12}\text{C}(p, p)^{12}\text{C}$ differential cross section, as the thickness of carbon and boron in the targets had been previously measured, Sec. II B. Taking the uncertainty in the carbon target thickness (5%), the uncertainty in the boron target thickness of (6%), the systematic uncertainty from Meyer *et al.* [48] and an estimated 5% interpolation uncertainty from the R -matrix calculation, this normalization procedure contributes an estimated 10% to the systematic uncertainty budget.

Targets were tested for deterioration throughout the experiment by making repeated runs at the same energies to check for consistent yields. No measurable target degradation was observed. This was expected as the targets used at Ohio University were about an order of magnitude thicker than those used in the Notre Dame measurement and no degradation was observed. In addition, beam intensities used at Ohio University were less than those used at Notre Dame. As a further check, repeated measurements were made at several energies throughout the experiment, and consistent yields were obtained. Therefore, no additional uncertainty was included for target degradation for this portion of the experiment.

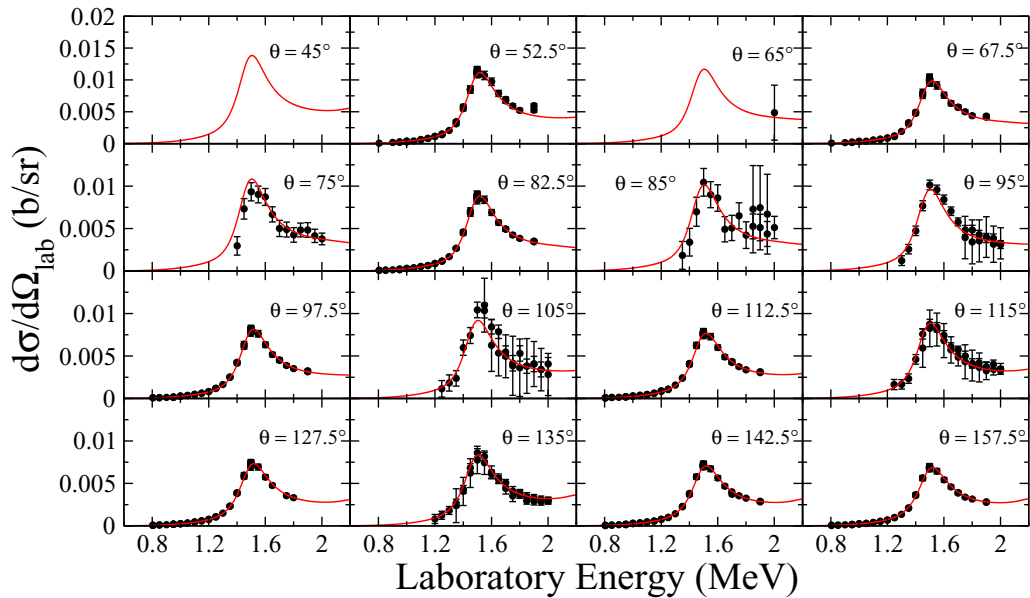
Differential cross sections were determined using the thin target approximation given by Eq. (1). While the target used for the Ohio University experiments was approximately an order of magnitude thicker than that used for the University of Notre Dame measurements, the thin target approximation

is still a good approximation. The proton energy loss through the boron target ranged from 13 keV at $E_p = 800$ keV to 7 keV at $E_p = 2$ MeV. The experimental data for both measurements can be found in the Supplemental Material [50] and are shown in Figs. 7 and 8. The systematic uncertainties are summarized in Table I.

IV. R -MATRIX ANALYSIS

One of the main difficulties encountered in the R -matrix fit of Wiescher *et al.* [21], was the lack of constraint on the position and width of the broad resonances that are the dominant contributors to the cross sections of the $^{10}\text{B}(p, \alpha_0)^7\text{Be}$ and $^{10}\text{B}(p, \alpha_1)^7\text{Be}$ reactions over the range from $E_{c.m.} \approx 1$ to 2 MeV. The new data presented here were measured specifically to remedy this issue, and, as will be shown, they largely do so. The R -matrix fits presented here were done in three parts. First, a fit to only the data from the present work and the $^{10}\text{B}(p, p)^{10}\text{B}$ data of Chiari *et al.* [51] was performed in order to focus on the region from $E_{c.m.} \approx 1$ to 2 MeV. Then the fit was extended to very low energies using a few representative data sets [21,28,30,39] in order find if a consistent fitting over the wider energy range could be achieved. Finally, the fit was further extended to the $^{10}\text{B}(p, \gamma)^{11}\text{C}$ data of Wiescher *et al.* [52], which has never been previously included in an R -matrix analysis.

In this work, cross sections are reported for the $^{10}\text{B}(p, \alpha_0)^7\text{Be}$ and $^{10}\text{B}(p, \alpha_1)^7\text{Be}$ reactions as these yields were observed to dominate over the entire energy range ($0.8 < E_p < 2.0$ MeV). However, the reactions $^{10}\text{B}(p, p_1)^{10}\text{B}$ and $^{10}\text{B}(p, ^3\text{He})^8\text{Be}$ are also energetically possible. Weak proton peaks corresponding to inelastic proton scattering were observed in some runs, but since their yields were


 FIG. 8. As Fig. 7, but for the $^{10}\text{B}(p, \alpha_1)^7\text{Be}$ reaction.

approximately an order of magnitude smaller than the $^{10}\text{B}(p, \alpha)^7\text{Be}$ reactions, the p_1 reaction channel is neglected in the R -matrix analysis. Likewise, no yields were observed for the $^{10}\text{B}(p, ^3\text{He})^8\text{Be}$, so the ^3He channel is also neglected.

For the R -matrix fits presented here, the code AZURE2 [49,53] has been used. The code uses the alternative R -matrix parametrization of Brune [54] to work directly with observed widths and energies and to remove the need for boundary conditions. This only leaves the channel radius model parameters, which were chosen as 5.0 fm for the proton channels and 5.5 fm for the α_0 and α_1 channels. Masses and particle separation energies were taken from the AME mass evaluations [55,56] and were treated as constants. The corrections due to energy loss through the target were performed using the experimental effect routine of AZURE2, where stopping powers were taken from the code SRIM-2013 [46].

A. Present data

As the present $^{10}\text{B}(p, \alpha_{0,1})^7\text{Be}$ data and the $^{10}\text{B}(p, p_0)^{10}\text{B}$ from Chiari *et al.* [51] provide comprehensive measurements over the energy range from $E_p = 0.8$ to 2.0 MeV for all of the dominant reaction channels, these data sets provide sufficient constraint for an initial multichannel R -matrix fit. Starting from the levels and their parameters listed in the most recent ENSDF evaluation [42], it was quickly apparent that the angular distributions of the $^{10}\text{B}(p, p_0)^{10}\text{B}$ and $^{10}\text{B}(p, \alpha_1)^7\text{Be}$ data could be reproduced, but those of the $^{10}\text{B}(p, \alpha_0)^7\text{Be}$ data could not.

In particular, the $^{10}\text{B}(p, p_0)^{10}\text{B}$ data can be well described by the $J^\pi = 7/2^+$ level at $E_x = 10.05$ MeV ($E_{c.m.} = 1.36$ MeV) and the $9/2^+$ level at $E_x = 10.71$ MeV ($E_{c.m.} = 2.02$ MeV), which are clearly visible resonances in the data. In addition, the near threshold $5/2^+$ level at $E_x = 8.699$ MeV and a high energy $5/2^+$ background level are also needed to reproduce the scattering cross sections. For the $^{10}\text{B}(p, \alpha_1)^7\text{Be}$

data, the $7/2^+$ level at $E_x = 10.05$ MeV ($E_{c.m.} = 1.36$ MeV) dominates the cross section. The $^{10}\text{B}(p, \alpha_0)^7\text{Be}$ differential cross sections were much more challenging to reproduce. From the experimental data at backward angles, it is clear that two resonances are present, one at $E_{c.m.} \approx 1.05$ MeV ($E_x = 9.74$ MeV) and another at $E_{c.m.} \approx 1.36$ MeV ($E_x = 9.74$ MeV). Moving forward in angle, the relative strength of the $E_{c.m.} \approx 1.05$ MeV resonance decreases compared to the $E_{c.m.} \approx 1.36$ MeV resonance, making the separation of the two resonances more difficult to identify. This was previously observed in the measurements of Brown *et al.* [24] and Cronin [26].

The identification of the spin-parity of the levels that correspond to these two broad resonances is obfuscated by the strong interference between not only these two resonances, but also the underlying tails of other broad resonances at both higher and lower energies. In particular, the interference pattern between the two resonances was very challenging to reproduce simultaneously at all angles. This is further complicated because the spin of ^{10}B is 3^+ . This means that there are often multiple channel spins (s) and/or relative orbital angular momentum (ℓ) channels that are possible for each level and multiple J^π that are populated with the same ℓ for the $^{10}\text{B} + p$ particle partition. For example, both $3/2^+$ and $1/2^+$ levels can be populated through $\ell = 2$, and for $3/2^+$, there are two possible channels, for channel spins $5/2$ and $7/2$. The fitting is made further challenging because depending on the particular channels used, or combinations of channels, differences in the angular distributions can be produced. These differences are at a level that is often similar to the uncertainties in the data, making discerning the correct solution quite challenging. The multichannel R -matrix fit, at representative angles, is shown in Fig. 9.

B. Extension to low energy

The R -matrix fit to data of just this work (Sec. IV A) was then expanded to the low energy range using a few

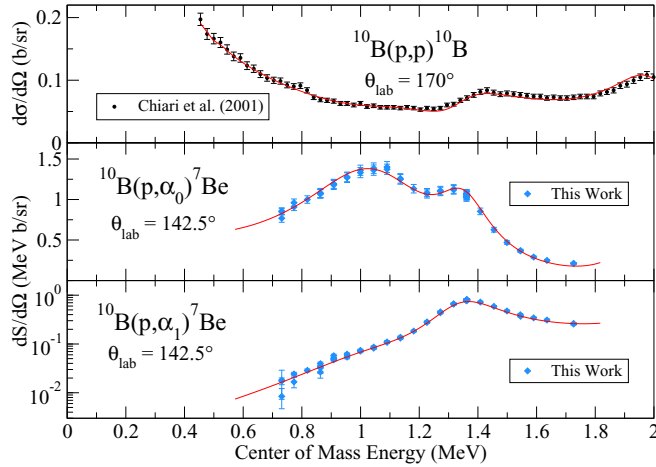


FIG. 9. *R*-matrix fit, shown at representative angles, to the present $^{10}\text{B}(p, \alpha_0)^7\text{Be}$ and $^{10}\text{B}(p, \alpha_1)^7\text{Be}$ data as well as the $^{10}\text{B}(p, p_0)^{10}\text{B}$ data of Chiari *et al.* [51].

representative data sets [21,28,30,39]. These data were found to be generally in agreement with the present measurements in the region of overlap (see Fig. 10). The exception are the $^{10}\text{B}(p, \alpha_1)^7\text{Be}$ data of Wiescher *et al.* [21], which deviated substantially from the present measurements. At $E_{c.m.} > 1.0$ MeV, the data are in excellent agreement with the present measurements if they are renormalized by a factor of 0.6. At higher energies, the data become suddenly quite inconsistent in their energy dependence as well. In light of this discrepancy, a re-examination of the data of Wiescher *et al.* [21] found that the data were measured at different experimental facilities, which may have introduced a systematic error in the high energy data taken at the Ohio State CN VdG facility

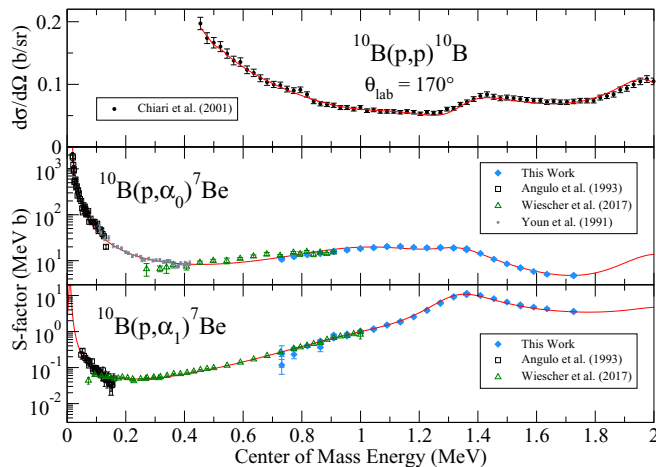


FIG. 10. *R*-matrix fit extended to low energy. The fit included the present data for the $^{10}\text{B}(p, \alpha_0)^7\text{Be}$ and $^{10}\text{B}(p, \alpha_1)^7\text{Be}$ reactions as well as the lower energy data sets of Angulo *et al.* [30] Angulo *et al.* [39], Wiescher *et al.* [21], and Youn *et al.* [28], and the $^{10}\text{B}(p, p_0)^{10}\text{B}$ data of Chiari *et al.* [51]. The fit was made directly to the differential cross section data of the present measurement, but the data were angle integrated for visual comparison with the other angle-integrated data sets.

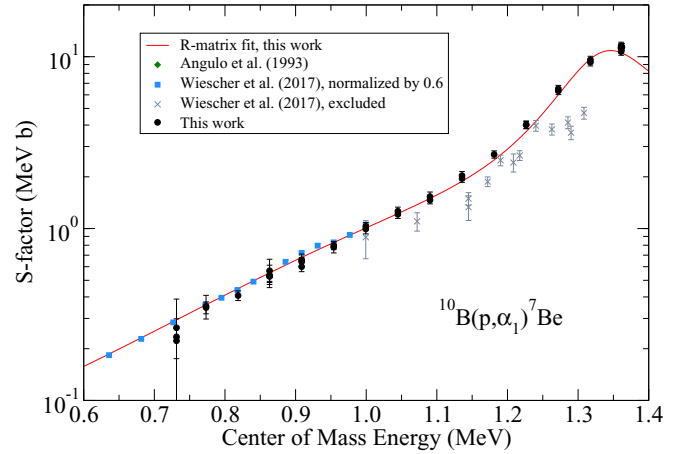


FIG. 11. Comparison of the $^{10}\text{B}(p, \alpha_1)^7\text{Be}$ data (black circles) and *R*-matrix fit (red line) from the present work with the data of Wiescher *et al.* [21]. At $E_{c.m.} < 1.0$ MeV, the data of Wiescher *et al.* [21] are in good agreement with the present measurements if they are renormalized by a factor of 0.6 (blue squares). At higher energies, it is recommended that the data of Wiescher *et al.* [21] be excluded, as they deviate from the present measurements in energy dependence as well. See text for details.

under very limited beam current conditions. These data were therefore discarded from the analysis, as indicated in Fig. 11.

Unfortunately, these types of data inconsistencies are quite common in the literature data, as mentioned in Sec. I and as highlighted in Wiescher *et al.* [21]. This is why this preliminary fit to higher energies is limited to only a few data sets, and even among those, inconsistencies can be seen in some overlapping regions. The consistency achieved between the two independent measurements presented in this work provide additional confidence in their accuracy. These issues will be discussed further in Sec. V.

C. Extension to capture

In order to check the consistency with the present fit to the radiative capture data of Wiescher *et al.* [52], the primary transition cross sections were investigated. The data were not available in tabular form and were obtained from the EXFOR database [57], where the data had been digitized from Fig. 5 of Wiescher *et al.* [52]. A more limited fit was performed where the particle widths were held fixed to the values obtained from the fit to the particle data, and only the γ -ray partial widths and asymptotic normalization coefficients were allowed to vary. It was found that a good reproduction of the capture data of Wiescher *et al.* [52] could be achieved, but with this more limited set of positive parity levels as shown in Fig. 12. For the data of Wiescher *et al.* [52], target effect corrections were found to be quite significant. Calculations of both the experimental effects corrected and bare *R*-matrix *S* factors are shown in Fig. 12.

In this work, only the capture *S* factors for the three transitions that have significant resonance contributions were investigated (ground state, third, and fifth excited states). It was found that the dominant resonance contributions came

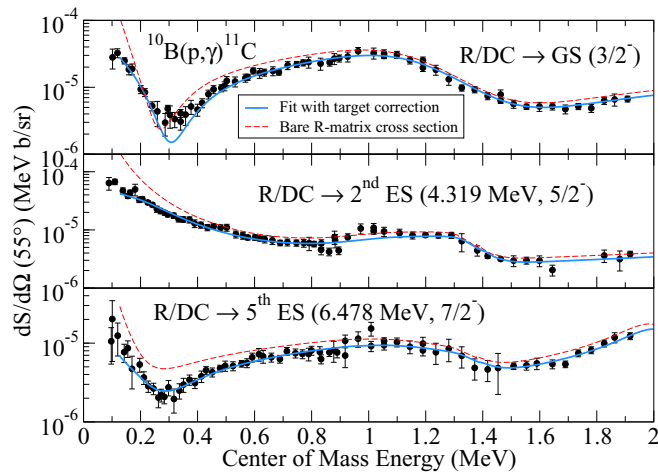


FIG. 12. S factors showing the R -matrix fit to the primary-transition capture data of Wiescher *et al.* [52] that contain significant resonance contributions. The blue solid line represents the R -matrix S factor corrected for the experimental target effects quoted in Wiescher *et al.* [52], while the red dashed line represents the bare R -matrix S factor.

from the levels corresponding to the near threshold ($E_x = 8.699$ MeV, $E_{c.m.} = 0.01$ MeV) and that at $E_x = 9.96$ MeV ($E_{c.m.} = 1.27$ MeV), both of which are $5/2^+$ levels with incoming angular momentum $\ell = 0$. External capture contributions were also found to be significant for all three transitions. The only region of the capture data that was not well fit was in the transition to the third excited state in the energy region around $E_{c.m.} \approx 1$ MeV ($E_x \approx 9.69$ MeV) (see Fig. 12), where there seems to be an additional resonance contribution. Thus, there remains the possibility that an additional level could be present in this region.

V. DISCUSSION

In Wiescher *et al.* [21] (Fig. 9), the discrepancies between different previous measurements of the $^{10}\text{B}(p, \alpha)^7\text{Be}$ reaction were highlighted, in particular the ground state transition. It was also shown how these discrepancies led to large variations in the R -matrix fits reported recently [21,31,60]. These previous R -matrix calculations of the S factors are compared in Fig. 13, along with that of the present work.

The present data indicate less underlying structure than previously proposed. In particular, Wiescher *et al.* [52] proposed that three negative parity states are present between the proton threshold and $E_x = 10$ MeV. The combination of inconsistent $^{10}\text{B}(p, \alpha)^7\text{Be}$ data and the inclusion of these states, led to an overfitting of the data and to the more oscillatory S factors compared to the present calculation as shown in Fig. 13. Table II summarizes the levels reported in the ENSDF evaluation [42] that were not needed to describe the data in the present analysis. This reduction in levels and the improved energy and angular coverage of the present data has led to a significant reduction in the uncertainty of the cross section over the energy range of the present data ($0.8 < E_p < 2.0$ MeV). Variations of up to 50% have been shown to be present

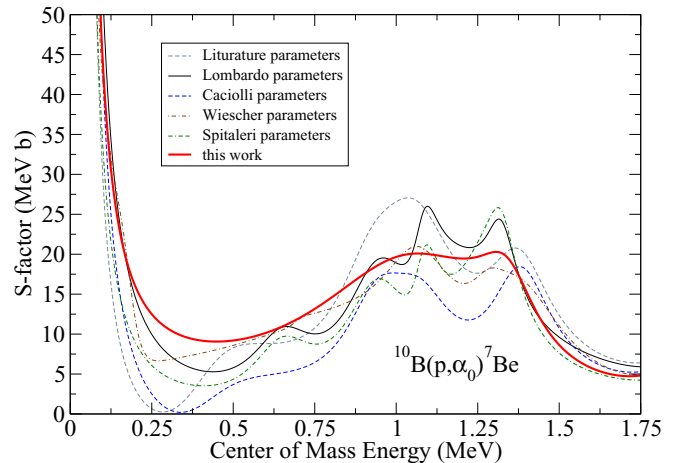


FIG. 13. Comparison of S factors determined from recent R -matrix fits by Lombardo *et al.* [31] (black solid line), Cacioli *et al.* [60] (blue dashed line), and Wiescher *et al.* [21] (brown dotted-dashed line), Spitaleri *et al.* [36] (green dashed-dashed-dotted line) using level parameters from the ENSDF evaluation [42] (grey dashed line) and the present work (red solid line).

between recent R -matrix fits that cover this energy range. Compared to the recent evaluation by Wiescher *et al.* [21], deviations as large as 20% exist. The present measurements reduce the uncertainty in this region to the 10–12% level, that is, that of the dominant systematic uncertainties (see Table I).

In addition to fewer levels, the present fit also favored a change in the spin-parity assignment for the low-lying broad resonance from $5/2^+$ to $3/2^+$. While the width obtained here is similar to that quoted in the ENSDF evaluation [42], the energy is significantly higher, as summarized in Table III. For the $7/2^+$ and $9/2^+$ levels at $E_x = 10.05$ and 10.7 MeV, it is suggested that the tentative spin-parity assignments in the compilation be changed to firm assignments, as they are uniquely constrained by the scattering data of [51]. Different spin-parity combinations were investigated in the present work and only the suggested ones were found to reproduce the angular distributions of both the $^{10}\text{B}(p, \alpha)^7\text{Be}$ and $^{10}\text{B}(p, p)^{10}\text{B}$ data simultaneously.

For the reasons discussed in Sec. I, there are limited previous measurements over the energy range of this study that the present data can be compared to directly. The only two available are those of Brown *et al.* [24] (1951) and Cronin [26] (1956). As shown in Fig. 14, the present data are generally consistent with those of Cronin [26], both the excitation functions and angular distributions. This is also true for the $^{10}\text{B}(p, \alpha_1)^7\text{Be}$ data of Brown *et al.* [24], but their

TABLE II. Summary of levels reported in the ENSDF evaluation [42] but found not to be needed in the R -matrix description of the present data.

J^π	E_x	Γ_{total}
$(3/2^-)$	9.645(50)	210(40)
$(5/2^-)$	9.780(50)	240(50)
$(7/2^-)$	9.970(50)	120(20)

TABLE III. R -matrix parameters for the analysis of the ^{11}C system. The partial widths are in units of keV and excitation energies in MeV. The sign of the partial width indicates the interference sign of the corresponding reduced width amplitude. Parameters that were varied in the fitting are marked in **bold**. The level parameter uncertainties were estimated using codes BRICK [58] and EMCEE [59]. Some level parameters have been reported previously in the literature and are compared using the format (this work/ENSDF evaluation [42]).

J^π	E_x	this work/ENSDF evaluation [42]					
		s	l	Γ_{p0}	$\Gamma_{\alpha 0}$	$\Gamma_{\alpha 1}$	Γ_{total}
$5/2^+ / 5/2^+$	8.6987/8.699(2)	5/2	0	$2.5^{+1.2}_{-1.1} \times 10^{-17}$	15	$-17^{+1}_{-1} \times 10^{-3}$	15(1)
		3/2	1				
		1/2	3				
$(3/2^+) / 5/2^+$	$9.744^{+0.011}_{-0.008} / 9.20(5)$	5/2	0	$13.4^{+4.4}_{-2.5}$	430^{+180}_{-190}	491.6/500(90)	
		3/2	1				
		1/2	3				
$(5/2^+)$	$9.962^{+0.013}_{-0.006}$	5/2	0	124^{+6}_{-5}	565^{+27}_{-29}	740	
		3/2	1				
		1/2	3				
$7/2^+ / (7/2^+)$	$10.0465^{+0.0011}_{-0.0011} / 10.083(5)$	7/2	0	$52.6^{+1.7}_{-1.8}$	$58.4^{+2.4}_{-2.3}$	218/230(20)	
		3/2	3				
		1/2	3				
$9/2^+ / (9/2^+)$	$10.7123^{+0.0015}_{-0.0017} / 10.679(5)$	5/2	2	$-34.3^{+8.5}_{-12.4}$ $-114^{+2.3}_{-2.4}$	72^{+22}_{-18}	250/200(30)	
		7/2	2				
		3/2	3				
		1/2	5				
$(7/2^+)^a$	11.44 / 11.44(1)	7/2	0	1260^{+60}_{-70}	$-30.0^{+2.0}_{-2.5}$	740	
		1/2	3				
$5/2^+{}^a$	15	5/2	0	8400^{+400}_{-400}	-213^{+16}_{-17}	740	
		3/2	1				

^aThe $7/2^+$ and $5/2^+$ energy levels at 11.44 MeV and 15 MeV, respectively, are background levels.

$^{10}\text{B}(p, \alpha_0)^7\text{Be}$ have a somewhat different energy dependence than those of the present study. The sparsity of both data sets and the inconsistent data of Brown *et al.* [24] complicated the fitting described in Wiescher *et al.* [21], motivating the present measurements.

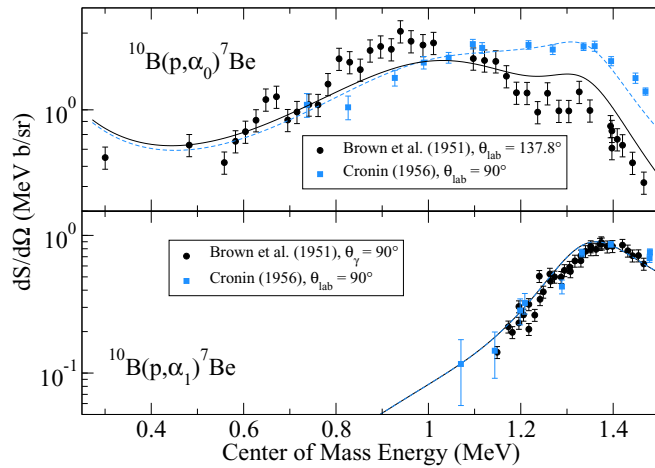


FIG. 14. Comparison of the R -matrix fit to the data of the present work (solid and dashed lines) to the data of Brown *et al.* [24] and Cronin [26]. Note that the cross sections of Brown *et al.* [24] were determined through the detection of 429 keV isotropic secondary γ rays, while those of Cronin [26] were through α -particle detection.

Figure 15 compares the $^{11}\text{B}(p, \alpha)^8\text{Be}$ and $^{10}\text{B}(p, \alpha)^7\text{Be}$ data sets over the energy range pertinent for aneutronic fusion (see Sec. I). For the $^{11}\text{B}(p, \alpha)^8\text{Be}$ reaction, the first excited state transition dominates the total cross section over this energy range. For the $^{10}\text{B}(p, \alpha)^7\text{Be}$ reaction, the $^{10}\text{B}(p, \alpha_0)^7\text{Be}$ transition dominates at low energies, but the $^{10}\text{B}(p, \alpha_1)^7\text{Be}$

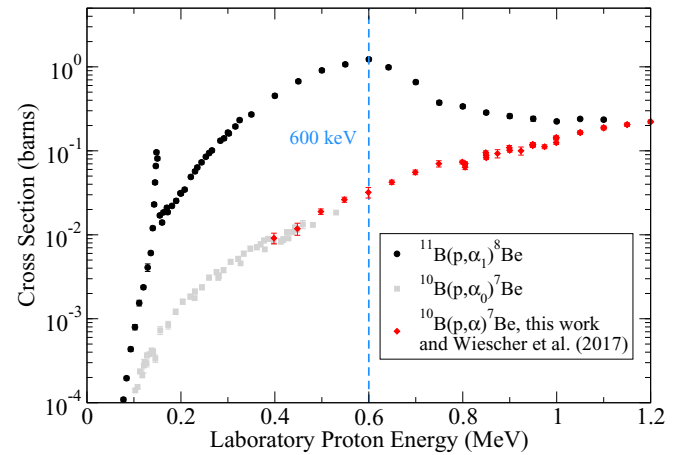


FIG. 15. Comparison of the $^{11}\text{B}(p, \alpha)^8\text{Be}$ [14] (black circles) and $^{10}\text{B}(p, \alpha)^7\text{Be}$ [21,28,30] (grey squares) cross section data over the energy range of interest for aneutronic fusion applications. The present $^{10}\text{B}(p, \alpha)^7\text{Be}$ total cross section data are indicated by the red diamonds.

transition begins to make a substantial contribution to the total at $E_p \approx 1$ MeV. In Fig. 15, the sum of the present $^{10}\text{B}(p, \alpha_0)^7\text{Be}$ and $^{10}\text{B}(p, \alpha_1)^7\text{Be}$ data have been taken and the total $^{10}\text{B}(p, \alpha)^7\text{Be}$ cross section is shown. While the $^{11}\text{B}(p, \alpha)^8\text{Be}$ cross section is much larger than that of the $^{10}\text{B}(p, \alpha)^7\text{Be}$ reaction over most of the energy range, the two become comparable at $E_p \approx 1$ MeV.

Finally, while the current measurements do not reach down into the low energy range needed for laser-driven, hot plasma facilities (≈ 10 keV), they provide much more stringent constraints on the background contributions for future phenomenological R -matrix analyses that will be used to evaluate lower energy measurements. The present measurements can also provide a check on the overall normalization of these lower energy studies, where an absolute normalization can be more challenging, if they extend high enough in energy to overlap. This is especially important for THM measurements, which have to be normalized to higher energy data, as they lack their own independent normalization. For the $^{10}\text{B}(p, \alpha)^7\text{Be}$ reaction, the THM measurements [33–36] are the only data that scan over the near threshold resonance that dominates the low energy cross section.

A comprehensive re-evaluation of the very low energy cross section is beyond the scope of this work. While the present data are a step forward in this effort, large inconsistencies are present in the currently available low energy data [21], which means that a re-evaluation with this same data would likely not result in a significant decrease in the uncertainty. Therefore, a consistent set of new low energy measurements is called for, at which point, they can be combined with the present work to produce an improved evaluation of the low energy $^{10}\text{B}(p, \alpha)^7\text{Be}$ reaction.

VI. SUMMARY

The $^{10}\text{B}(p, \alpha)^7\text{Be}$ reaction is a potential diagnostic reaction for aneutronic fusion and laser-driven, hot-plasma facilities. However, despite a large amount of experimental

data, the cross section was quite uncertain because of conflicting measurements and a lack of measurements of certain energy and angular ranges. In the present work, new measurements have been performed for the $^{10}\text{B}(p, \alpha)^7\text{Be}$ reaction, clearly discriminating the $^{10}\text{B}(p, \alpha_0)^7\text{Be}$ and $^{10}\text{B}(p, \alpha_1)^7\text{Be}$ yields from the elastic scattering yields using either degrader foil or time-of-flight techniques. The resulting differential cross sections cover an experimentally challenging energy region from $E_p = 0.8$ to 2 MeV with greater energy and angular coverage and smaller uncertainties. The new data have enabled a much more confident R -matrix description of not only the $^{10}\text{B}(p, \alpha_0)^7\text{Be}$, $^{10}\text{B}(p, \alpha_1)^7\text{Be}$, and $^{10}\text{B}(p, p)^{10}\text{B}$ cross sections, resolving discrepancies between previous data sets, but also provided a consistent description of the $^{10}\text{B}(p, \gamma)^{11}\text{C}$ data for the first time. It was found that the $^{10}\text{B}(p, \alpha)^7\text{Be}$ and $^{10}\text{B}(p, \gamma)^{11}\text{C}$ data could be described with only the positive parity states reported previously in the literature, which has shed light on the fitting inconsistencies observed in other recent R -matrix analyses. The present data thus reduce the uncertainty in the cross section over the energy range important for aneutronic fusion (200 to 1000 keV) and set the stage for a new R -matrix evaluation of the ^{11}C system, paving the way for an improved determination of the very low energy (≈ 10 keV) cross-section region needed for laser-driven fusion applications.

ACKNOWLEDGMENTS

We would like to acknowledge Aurora Tumino and Gianluca Imbriani for their help with boron target development. This research utilized resources from the Notre Dame Center for Research Computing and was supported by the National Science Foundation through Grant No. Phys-2011890, and the Joint Institute for Nuclear Astrophysics through Grant No. PHY-1430152 (JINA Center for the Evolution of the Elements).

-
- [1] R. Feldbacher and M. Heindler, Basic cross section data for aneutronic reactor, *Nucl. Instrum. Methods Phys. Res. A* **271**, 55 (1988).
- [2] W. Nevins and R. Swain, The thermonuclear fusion rate coefficient for p- ^{11}B reactions, *Nucl. Fusion* **40**, 865 (2000).
- [3] R. Kouzes, The ^3He Supply Problem., Technical Report No. PNNL-18388 (Pacific Northwest National Laboratory, Richland, WA, 2009).
- [4] J. Treglio, Conditions for a boron fusion reactor in the mev range, *Nucl. Instrum. Methods* **144**, 65 (1977).
- [5] J. Dawson, Plasma Physics Group Report PPG-273, University of California: CTR using the p-B11 reaction (1976).
- [6] Y. Matsumoto, T. Nagaura, Y. Itoh, S. Oikawa, and T. Watanabe, Lhd type proton-boron reactor and the control of its peripheral potential structure, *J. Plasma Fusion Res.* **4**, 422 (2001).
- [7] N. Rostoker, M. W. Binderbauer, and H. J. Monkhorst, Colliding beam fusion reactor, *Science* **278**, 1419 (1997).
- [8] V. S. Belyaev, A. P. Matafonov, V. I. Vinogradov, V. P. Krainov, V. S. Lisitsa, A. S. Roussetski, G. N. Ignatyev, and V. P. Adrianov, Observation of neutronless fusion reactions in picosecond laser plasmas, *Phys. Rev. E* **72**, 026406 (2005).
- [9] H. Hora, G. Miley, N. Azizi, B. Malekynia, M. Ghoranneviss, and X. He, Nonlinear force driven plasma blocks igniting solid density hydrogen boron: Laser fusion energy without radioactivity, *Laser Part. Beams* **27**, 491 (2009).
- [10] H. Hora, G. Miley, K. Flippo, P. Lalouis, R. Castillo, X. Yang, B. Malekynia, and M. Ghoranneviss, Review about acceleration of plasma by nonlinear forces from picosecond laser pulses and block generated fusion flame in uncompressed fuel, *Laser Part. Beams* **29**, 353 (2011).
- [11] I. Last, S. Ron, and J. Jortner, Aneutronic $\text{h} + ^{11}\text{B}$ nuclear fusion driven by coulomb explosion of hydrogen nanodroplets, *Phys. Rev. A* **83**, 043202 (2011).
- [12] G. A. Mourou, C. P. J. Barty, and M. D. Perry, Ultrahigh-intensity lasers: Physics of the extreme on a tabletop, *Phys. Today* **51**, 22 (1998).
- [13] P. Lalouis, H. Hora, S. Eliezer, J.-M. Martinez-Val, S. Moustazis, G. H. Miley, and G. Mourou, Shock mechanisms

- by ultrahigh laser accelerated plasma blocks in solid density targets for fusion, *Phys. Lett. A* **377**, 885 (2013).
- [14] H. W. Becker, C. Rolfs, and H. P. Trautvetter, Low-energy cross sections for $^{11}\text{B}(p, 3\alpha)$, *Z. Phys. A* **327**, 341 (1987).
- [15] V. S. Belyaev, V. I. Vinogradov, A. P. Matafonov, S. M. Rybakov, V. P. Krainov, V. S. Lisitsa, V. P. Andrianov, G. N. Ignatiev, V. S. Bushuev, A. I. Gromov, A. S. Rusetsky, and V. A. Dravin, Excitation of promising nuclear fusion reactions in picosecond laser plasmas, *Phys. At. Nucl.* **72**, 1077 (2009).
- [16] C. N. Davids, A. J. Elwyn, B. W. Filippone, S. B. Kaufman, K. E. Rehm, and J. P. Schiffer, Branching ratio in the electron-capture decay of ^7Be , *Phys. Rev. C* **28**, 885 (1983).
- [17] N. Otuka, E. Dupont, V. Semkova, B. Pritychenko, A. Blokhin, M. Aikawa, S. Babykina, M. Bossant, G. Chen, S. Dunaeva, R. Forrest, T. Fukahori, N. Furutachi, S. Ganesan, Z. Ge, O. Gritzay, M. Herman, S. Hlavač, K. Katō, B. Lalremruata *et al.*, Towards a more complete and accurate experimental nuclear reaction data library (EXFOR): International collaboration between nuclear reaction data centres (NRDC), *Nucl. Data Sheets* **120**, 272 (2014).
- [18] W. Hogan, E. Moses, B. Warner, M. Sorem, and J. Soures, The national ignition facility, *Nucl. Fusion* **41**, 567 (2001).
- [19] M. J. Guardalben, M. Barczys, B. E. Kruschwitz, M. Spilatro, L. J. Waxer, and E. M. Hill, Laser-system model for enhanced operational performance and flexibility on omega ep, *High Power Laser Science and Engineering* **8**, e8 (2020).
- [20] R. Hatarik, D. B. Sayre, J. A. Caggiano, T. Phillips, M. J. Eckart, E. J. Bond, C. Cerjan, G. P. Grim, E. P. Hartouni, J. P. Knauer, J. M. McNaney, and D. H. Munro, Analysis of the neutron time-of-flight spectra from inertial confinement fusion experiments, *J. Appl. Phys.* **118**, 184502 (2015).
- [21] M. Wiescher, R. J. deBoer, J. Görres, and R. E. Azuma, Low energy measurements of the $^{10}\text{B}(p, \alpha)^7\text{Be}$ reaction, *Phys. Rev. C* **95**, 044617 (2017).
- [22] W. Burcham and J. M. Freeman, LXXVI. The emission of short-range alpha particles from light elements under proton bombardment. I. Experimental method and the reaction $^{10}\text{B}(p, \alpha)^7\text{Be}$, *The London, Edinburgh, and Dublin Philosophical Magazine and Journal of Science* **40**, 807 (1949).
- [23] W. Burcham and J. M. Freeman, XXVII. The emission of short-range alpha particles from light elements under proton bombardment. II. Further observations on the reaction $^{10}\text{B}(p, \alpha)^7\text{Be}$, *The London, Edinburgh, and Dublin Philosophical Magazine and Journal of Science* **41**, 337 (1950).
- [24] A. B. Brown, C. W. Snyder, W. A. Fowler, and C. C. Lauritsen, Excited states of the mirror nuclei, Li^7 and Be^7 , *Phys. Rev.* **82**, 159 (1951).
- [25] G. Bach and D. Livesey, XCIII. The cross section for the reaction $^{10}\text{B}(p, \alpha)^7\text{Be}$ at proton energies below 200 keV, *The London, Edinburgh, and Dublin Philosophical Magazine and Journal of Science* **46**, 824 (1955).
- [26] J. W. Cronin, Excitation functions and angular distributions of alpha particles leading to the ground and first excited states of Be^7 in the reaction $\text{B}^{10}(p, \alpha)\text{Be}^{7*}$, *Phys. Rev.* **101**, 298 (1956).
- [27] J. Szabó, J. Csikai, and M. Várnagy, Low-energy cross sections for $^{10}\text{B}(p, \alpha)^7\text{Be}$, *Nucl. Phys. A* **195**, 527 (1972).
- [28] M. Youn, H. Chung, J. Kim, H. Bhang, and K.-H. Chung, The $^{10}\text{B}(p, \alpha_0)^7\text{Be}$ reaction in the thermonuclear energy region, *Nucl. Phys. A* **533**, 321 (1991).
- [29] F. Knappe, H. Bucka, and P. Heide, in *The $^{10}\text{B}(p, \alpha_0)^7\text{Be}$ reaction at thermonuclear energies*, in *Nuclei in the Cosmos 2*, edited by F. Kaeppler and K. Wisshak (IOP Publishing, Bristol, UK, 1993), pp. 175–180.
- [30] C. Angulo, S. Engstler, G. Raimann, C. Rolfs, W. H. Schulte, and E. Somorjai, The effects of electron screening and resonances in (p, α) reactions on ^{10}B and ^{11}B at thermal energies, *Z. Phys. A* **345**, 231 (1993).
- [31] I. Lombardo, D. Dell'Aquila, F. Conte, L. Francalanza, M. L. Cognata, L. Lamia, R. L. Torre, G. Spadaccini, C. Spitaleri, and M. Vigilante, New investigations of the $^{10}\text{B}(p, \alpha_0)^7\text{Be}$ reaction at bombarding energies between 0.6 and 1 MeV, *J. Phys. G: Nucl. Part. Phys.* **43**, 045109 (2016).
- [32] D. Dell'Aquila, Experimental studies of clustering in light nuclei: $^{11,12,13,16}\text{C}$, *Eur. Phys. J. Plus* **135**, 165 (2020).
- [33] L. Lamia, S. Romano, N. Carlin, S. Cherubini, V. Crucillà, M. D. Moura, M. D. Santo, M. Munhoz, M. Gulino, R. L. Neto, M. L. Cognata, F. Mudò, R. Pizzone, S. Puglia, M. Sergi, F. Souza, C. Spitaleri, A. Suaide, E. Szanto, A. S. de Toledo *et al.*, Boron depletion: Indirect measurement of the $^{10}\text{B}(p, \alpha)^7\text{Be}$ $S(E)$ -factor, *Nucl. Phys. A* **787**, 309 (2007).
- [34] L. Lamia, S. Puglia, C. Spitaleri, S. Romano, M. G. D. Santo, N. Carlin, M. G. Munhoz, S. Cherubini, G. Kiss, V. Kroha, S. Kubono, M. L. Cognata, C.-B. Li, R. Pizzone, Q.-G. Wen, M. Sergi, A. S. de Toledo, Y. Wakabayashi, H. Yamaguchi, and S.-H. Zhou, Indirect study of $^{11}\text{B}(p, \alpha_0)^8\text{Be}$ and $^{10}\text{B}(p, \alpha)^7\text{Be}$ reactions at astrophysical energies by means of the Trojan horse method: Recent results, *Nucl. Phys. A* **834**, 655c (2010).
- [35] C. Spitaleri, L. Lamia, S. M. R. Puglia, S. Romano, M. La Cognata, V. Crucillà, R. G. Pizzone, G. G. Rapisarda, M. L. Sergi, M. G. Del Santo, N. Carlin, M. G. Munhoz, F. A. Souza, A. Szanto de Toledo, A. Tumino, B. Irgaziev, A. Mukhamedzhanov, G. Tabacaru, V. Burjan, V. Kroha *et al.*, Measurement of the 10 keV resonance in the $^{10}\text{B}(p, \alpha_0)^7\text{Be}$ reaction via the Trojan horse method, *Phys. Rev. C* **90**, 035801 (2014).
- [36] C. Spitaleri, S. M. R. Puglia, M. La Cognata, L. Lamia, S. Cherubini, A. Cvetinović, G. D'Agata, M. Gulino, G. L. Guardo, I. Indelicato, R. G. Pizzone, G. G. Rapisarda, S. Romano, M. L. Sergi, R. Spartá, S. Tudisco, A. Tumino, M. G. Del Santo, N. Carlin, M. G. Munhoz *et al.*, Measurement of the $^{10}\text{B}(p, \alpha_0)^7\text{Be}$ cross section from 5 keV to 1.5 MeV in a single experiment using the Trojan horse method, *Phys. Rev. C* **95**, 035801 (2017).
- [37] R. B. Day and T. Huus, Gamma radiation from B^{10} bombarded by protons, *Phys. Rev.* **95**, 1003 (1954).
- [38] S. E. Hunt, R. A. Pope, and W. W. Evans, Investigation of the gamma radiation produced by irradiating B^{10} with protons in the energy range 0.7 to 3.0 MeV, *Phys. Rev.* **106**, 1012 (1957).
- [39] C. Angulo, W. H. Schulte, D. Zahnow, G. Raimann, and C. Rolfs, Astrophysical $S(E)$ factor of $^{10}\text{B}(p, \alpha_1)^7\text{Be}$ at low energies, *Z. Phys. A* **345**, 333 (1993).
- [40] A. M. Lane and R. G. Thomas, R -matrix theory of nuclear reactions, *Rev. Mod. Phys.* **30**, 257 (1958).
- [41] P. Descouvemont and D. Baye, The R -matrix theory, *Rep. Prog. Phys.* **73**, 036301 (2010).
- [42] J. Kelley, E. Kwan, J. Purcell, C. Sheu, and H. Weller, Energy levels of light nuclei $A = 11$, *Nucl. Phys. A* **880**, 88 (2012).
- [43] B. Vande Kolk, Cross section measurements of $^{10}\text{B}(p, \alpha)^7\text{Be}$, Ph.D. thesis, University of Notre Dame, 2021.
- [44] A. Antilla, J. Keinonen, M. Hautala, and I. Forsblom, Use of the $^{27}\text{Al}(p, \gamma)^{28}\text{Si}$, $E_p = 992$ keV resonance as a

- gamma-ray intensity standard, *Nucl. Instrum. Methods* **147**, 501 (1977).
- [45] R. Wheeler, Nuclear spectroscopy using charged particles, Ph.D. thesis, Ohio University, 2002.
- [46] J. F. Ziegler, M. D. Ziegler, and J. P. Biersack, SRIM - The stopping and range of ions in matter (2010), *Nucl. Instrum. Methods Phys. Res. B* **268**, 1818 (2010).
- [47] R. O. Nelson, E. G. Bilpuch, C. R. Westerfeldt, and G. E. Mitchell, Proton resonances in ^{28}Si from $E_x = 12.5$ to 13.4 mev, *Phys. Rev. C* **29**, 1656 (1984).
- [48] H. Meyer, G. Plattner, and I. Sick, Elastic $p + ^{12}\text{C}$ scattering between 0.3 and 2 MeV, *Z. Phys. A* **279**, 41 (1976).
- [49] R. E. Azuma, E. Uberseder, E. C. Simpson, C. R. Brune, H. Costantini, R. J. de Boer, J. Görres, M. Heil, P. J. LeBlanc, C. Ugalde, and M. Wiescher, AZURE: An R -matrix code for nuclear astrophysics, *Phys. Rev. C* **81**, 045805 (2010).
- [50] See Supplemental Material at <http://link.aps.org/supplemental/10.1103/PhysRevC.105.055802> for the experimental data and the AZURE2 input file from the R -matrix fit of this work.
- [51] M. Chiari, L. Giuntini, P. Mandò, and N. Taccetti, Proton elastic scattering cross-section on boron from 0.5 to 3.3 MeV, *Nucl. Instrum. Methods Phys. Res. B* **184**, 309 (2001).
- [52] M. Wiescher, R. N. Boyd, S. L. Blatt, L. J. Rybarczyk, J. A. Spizuoco, R. E. Azuma, E. T. H. Clifford, J. D. King, J. Görres, C. Rolfs, and A. Vlieks, ^{11}C level structure via the $^{10}\text{B}(p, \gamma)$ reaction, *Phys. Rev. C* **28**, 1431 (1983).
- [53] E. Uberseder and R. J. deBoer, AZURE User Manual (2015), azure.nd.edu.
- [54] C. R. Brune, Alternative parametrization of R -matrix theory, *Phys. Rev. C* **66**, 044611 (2002).
- [55] W. Huang, G. Audi, M. Wang, F. G. Kondev, S. Naimi, and X. Xu, The AME2016 atomic mass evaluation (I). Evaluation of input data and adjustment procedures, *Chin. Phys. C* **41**, 030002 (2017).
- [56] M. Wang, G. Audi, F. G. Kondev, W. Huang, S. Naimi, and X. Xu, The AME2016 atomic mass evaluation (II). Tables, graphs and references, *Chin. Phys. C* **41**, 030003 (2017).
- [57] V. Zerkin and B. Pritychenko, The experimental nuclear reaction data (EXFOR): Extended computer database and Web retrieval system, *Nucl. Instrum. Methods Phys. Res. A* **888**, 31 (2018).
- [58] D. Odell, C. R. Brune, D. R. Phillips, R. J. deBoer, and S. N. Paneru, Performing Bayesian analyses with AZURE2 using BRICK: an application to the ^7Be system, [arXiv:2112.12838](https://arxiv.org/abs/2112.12838).
- [59] D. Foreman-Mackey, D. W. Hogg, D. Lang, and J. Goodman, EMCEE: The MCMC Hammer, *Publ. Astron. Soc. Pac.* **125**, 306 (2013).
- [60] A. Caciolli, R. Depalo, C. Broggin, M. La Cognata, L. Lamia, R. Menegazzo, L. Mou, S. M. R. Puglia, V. Rigato, S. Romano, C. Rossi Alvarez, M. L. Sergi, C. Spitaleri, and A. Tumino, A new study of $^{10}\text{B}(p, \alpha)^7\text{Be}$ reaction at low energies, *Eur. Phys. J. A* **52**, 136 (2016).